Environmental Science & Technology

Article

Cite This: Environ. Sci. Technol. 2018, 52, 4285−4293

pubs.acs.org/est

# Porous Electrospun Fibers Embedding $TiO_2$ for Adsorption and Photocatalytic Degradation of Water Pollutants

Chang-Gu Lee,[†,‡,⊥] Hassan Javed,[†,‡,¶] Danning Zhang,[†,‡] Jae-Hong Kim,[†,§] Paul Westerhoff,[†,∥] Qilin Li,[†,‡] and Pedro J. J. Alvarez*[,†,‡]

[†]NSF Nanosystems Engineering Research Center for Nanotechnology Enabled Water Treatment (NEWT)

[‡]Department of Civil and Environmental Engineering, Rice University, Houston, Texas 77005, United States

[§]Department of Chemical and Environmental Engineering, Yale University, New Haven, Connecticut 06511, United States

[∥]School of Sustainable Engineering and the Built Environment, Arizona State University, Tempe, Arizona 85287, United States

Supporting Information

**ABSTRACT:** Using a bipolymer system consisting of polyvinylpyrrolidone (PVP) and poly(vinylidene fluoride) (PVDF), P25-$TiO_2$ was immobilized into thin film mats of porous electrospun fibers. Pores were introduced by dissolving sacrificial PVP to increase surface area and enhance access to $TiO_2$. The highest photocatalytic activity was achieved using a PVDF:PVP weight ratio of 2:1. Methylene blue (MB) was used to visualize contaminant removal, assess the sorption capacity (5.93 ± 0.23 mg/g) and demonstrate stable removal kinetics ($k_{MB}$ > 0.045 $min^{-1}$) under UVA irradiation (3.64 × $10^{-9}$ einstein/$cm^2$/s) over 10 cycles. Treatment was also accomplished via sequential MB sorption in the dark and subsequent photocatalytic degradation under UVA irradiation, to illustrate that these processes could be uncoupled to overcome limited light penetration. The photocatalytic mat degraded bisphenol A and 17$\alpha$-ethynylestradiol in secondary wastewater effluent (17 mg TOC/L), and (relative to $TiO_2$ slurry) immobilization of $TiO_2$ in the mat mitigated performance inhibition by co-occurring organics that scavenge oxidation capacity. This significantly lowered the electrical energy-per-order of reaction (EEO) needed to remove such endocrine disruptors in the presence of oxidant scavenging/inhibitory organics. Thus, effective $TiO_2$ immobilization into polymers with affinity toward specific priority pollutants could both increase the efficiency and reduce energy requirements of photocatalytic water treatment.


## INTRODUCTION

Photocatalytic water treatment achieves oxidative degradation (and potentially mineralization) of many priority organic pollutants using light irradiation without chemical addition. Titanium dioxide ($TiO_2$) is the most commonly used semiconductor photocatalyst due to its chemical resistance, mechanical robustness, and low cost.[1−3] $TiO_2$ nanoparticles are typically used as a suspended slurry.[4,5] Suspending nanoparticles by intense mixing can maximize light absorption and mass transfer, but requires an energy-intensive separation process such as membrane filtration for catalyst recovery. $TiO_2$ in general also exhibits low adsorption capacity toward priority organic pollutants, making it difficult to minimize reactive oxygen species (ROS) scavenging by background organic constituents in the bulk phase.[2,5−7] Alternatively, $TiO_2$ can be immobilized onto a larger substrate to avoid the costly separation step. Using an appropriate support material can also offer an opportunity to adsorb and bring priority pollutants near photocatalytic sites to more efficiently utilize the short-lived ROS (i.e., "bait-hook and destroy" strategy).[8] Several researchers have highlighted the benefits of coupling adsorption and photocatalytic degradation for effective removal of contaminants.[9−18]

Ideal substrate materials for photocatalyst immobilization should provide stable anchoring to prevent catalyst leaching, stability against ROS, and selective affinity toward target contaminants.[5] Various materials have been considered as photocatalyst supports, including glass, silica, ceramic, polymers, activated carbon, alumina, zeolite, and stainless steel.[5,6,19−21,54] Fluoropolymers such as polyvinylidene fluoride (PVDF) are promising substrates, since they offer high chemical and mechanical stability due to strong C−F bonds.[22] PVDF is also relatively inexpensive and readily available, which facilitates its use in diverse applications.[5,6] Furthermore, the hydrophobic nature of PVDF can allow nonpolar organic contaminants to concentrate on its surface where photocatalysts are anchored. The substrate architecture is also critical to provide high surface area. For polymeric materials, electrospinning is an appealing technique to fabricate ultrathin fibers with diameter of tens to hundreds of nm and relatively high surface area to anchor a large quantity of

Received: December 18, 2017
Revised: February 12, 2018
Accepted: March 19, 2018
Published: March 19, 2018





DOI: 10.1021/acs.est.7b06508
Environ. Sci. Technol. 2018, 52, 4285−4293

photocatalysts with minimal alteration of the fabrication process.[23] Electrospun PVDF nanofibers containing $TiO_2$ have been considered,[6,24] but preventing photocatalysts from being embedded inside the fibers—which results in loss of active catalyst surface—has been challenging.[2,23]

We here report novel PVDF fiber substrates that are made porous to significantly enhance water pollutant access to anchored $TiO_2$. Past studies have attempted to prepare porous fibers via phase separation and polymer blending methods.[25−27] The phase separation method introduces pores by evaporating volatile solvent during electrospinning, while the polymer blending method forms pores by removing one of the polymers from the electrospun fibers using post-treatment such as polymer dissolution. In this study, we blend PVDF with a water-soluble polymer, polyvinylpyrrolidone (PVP), prior to electrospinning; after fiber fabrication, PVP can be easily removed to form pores by simply washing it out with water.[26,27,53] While porous fibers have been used to anchor photocatalysts in the past,[23,28,29] electrospun fibers made of this particular polymer blend have not been used to anchor $TiO_2$. The performance and reusability of the mats made of porous PVDF fibers was assessed using methylene blue (MB) to facilitate comparison with other studies.[30−35,55] The capability of these mats to remove endocrine disruptors such as bisphenol A (BPA) and 17$\alpha$-ethynylestradiol (EE2) in wastewater treatment plant (WWTP) effluent was also investigated (as a tertiary treatment option) and compared to that of conventional $TiO_2$ slurry.

## MATERIALS AND METHODS

**Materials.** $TiO_2$ (Evonik P25, ≥ 99.5% purity), PVDF (MW = 534 000), PVP (MW = 40 000), *N*,*N*-dimethylacetamide (DMAc) (puriss. p.a., ≥ 99.5% purity), acetone (ACS reagent, ≥ 99.5% purity), acetonitrile (HPLC Plus, ≥ 99.9% purity), nitric acid (ACS reagent, 70% purity), MB (≥82% purity), BPA (≥99% purity), and EE2 (≥98% purity) were all obtained from Sigma-Aldrich. Hydrofluoric acid (48%, ACS reagent) and sulfuric acid (ACS reagent) were purchased from EMD Millipore Corporation. Deionized (DI) water (>18.2 MΩ) prepared by Millipore (Milli-Q Academic) water purification system was used for all dilutions and reagent preparation.

**Fabrication of Photocatalytic Electrospun Porous Fiber Mat with Embedded $TiO_2$.** PVDF and PVP were dissolved in DMAc/acetone (1:1 v:v) at various ratios (PVDF(wt %):PVP(wt %) = 18:0, 12:6, 9:9, and 6:12) along with 4 wt % $TiO_2$ to prepare electrospun fibers (EF) and electrospun porous fibers (EPF) with various compositions (Table 1). The solution was vigorously stirred at 60 °C for 1 h and cooled to room temperature prior to use. Electrospinning was conducted using a lab-scale setup consisting of a syringe pump and DC power supply (Figure 1(a)). The polymer solution was electrospun at an applied voltage of 12 kV and a flow rate of 0.3 mL/h using a 0.58 mm (ID) needle which was placed 15 cm apart from an aluminum foil connected to a counter electrode. After electrospinning for 10 h, the electrospun mat was immediately immersed in DI water, sonicated in a water bath (5510, Branson, USA) for 1 h, and placed at 60 °C for 24 h, to wash out PVP. The washed electrospun mat was dried in vacuum (Isotemp Model 281A, Fisher Scientific) at 90 °C for 18 h.

**Table 1. Synthesis Conditions and Naming of Electrospun Fibers (EF) and Electrospun Porous Fibers (EPF)**

| no. | polymer blending | $TiO_2$ concentration in polymer solution | sample name |
|---|---|---|---|
| 1 | PVDF (18%) | 0% | EF |
| 2 | PVDF (18%) | 4% | EF-$TiO_2$ |
| 3 | PVDF (12%)/PVP (6%) | 4% | EPF(2/1)-$TiO_2$ |
| 4 | PVDF (9%)/PVP (9%) | 4% | EPF(1/1)-$TiO_2$ |
| 5 | PVDF (6%)/PVP (12%) | 4% | EPF(1/2)-$TiO_2$ |

**Characterization of Electrospun Fiber Mat.** Scanning electron microscopy (SEM) images were obtained using Quanta 400F (FEI). Prior to SEM measurement, all samples were sputter coated (Desk V, Denton Vacuum) with gold to a thickness of 15 nm. Transmission electron microscopy (TEM) images were measured by a JEM-2010 High-resolution transmission electron microscope (JEOL). Water contact angles were measured using drop shape analyzer (DSA100, Krüss, Germany). Water droplets (3 $\mu$L) were placed on the sample surface and contact angle was measured at five different locations. Specific surface area and pore volume of the samples were measured using an Autosorb-3B (Quantachrome Instruments). Thermogravimetric analysis (TGA) was conducted using an SDT Q600 (TA Instruments) in an argon atmosphere (flow rate = 100 mL/min) at a ramping rate of 10 °C/min to 910 °C (see Supporting Information (SI) Text S1 and Figure S1). Fourier-transform infrared spectroscopy (FT-IR) was performed using a Thermo Scientific Nicolet iS50 (Thermo Scientific).

**Sorption and Photocatalytic Degradation Experiments.** As-prepared fiber mats were cut into 4 × 5 $cm^2$ rectangular coupons for the adsorption-photocatalytic degradation experiments (Figure 1(c)). A sample coupon was mounted on a steel wire frame and hung inside a quartz beaker (50 mL) (Figure 1(d)). The kinetics of MB (3.2 mg/L) adsorption to these coupons was first evaluated in the dark over 240 min. Experiments to evaluate the kinetics of MB removal by concurrent adsorption and photodegradation were then conducted in a black acrylic box (18 × 18 × 18 $cm^3$) equipped with six UVA lamps (F4T5/BLB, 4W, Eiko) (Figure 1(e)). The wavelength of UVA (mean $\lambda$ = 365 nm) was measured by a High-Resolution Spectrometer (HR4000, Ocean Optics) (SI Figure S2), and the photonic flux inside the photoreactor was assessed using potassium ferrioxalate actinometery[36] (see SI Text S2 and Figure S3 for details). For these tests, 50 mL of MB solution (6.4 mg/L) were irradiated for 120 min in a quartz beaker containing a hung fiber mat. The stability of the fiber mat was evaluated over 10 continuous cycles of 90 min UVA exposure. Another set of experiments was performed to uncouple adsorption and photocatalysis; by first performing adsorption in the dark for 240 min followed by photocatalytic degradation for 90 min under UVA exposure.

Experiments were also conducted to evaluate the ability of the EPF mat to remove select endocrine disrupting compounds (EDCs) under the condition that simulated WWTP effluent tertiary treatment, and to investigate the potential interference of background organic matter. BPA and EE2 ($C_0$ = 5.0 mg/L) were spiked in both DI water and the effluent from the West University Place WWTP in Houston, TX (TOC = 17 mg/L; SI Table S1) and subjected to concurrent adsorption and photocatalytic degradation as described above for 240 min.

**Analytical Methods.** MB concentration in water was measured by a UV−visible spectrophotometer (Ultrospec 2100 pro, Amersham Biosciences) at 664 nm. BPA and EE2 were


DOI: 10.1021/acs.est.7b06508
Environ. Sci. Technol. 2018, 52, 4285−4293

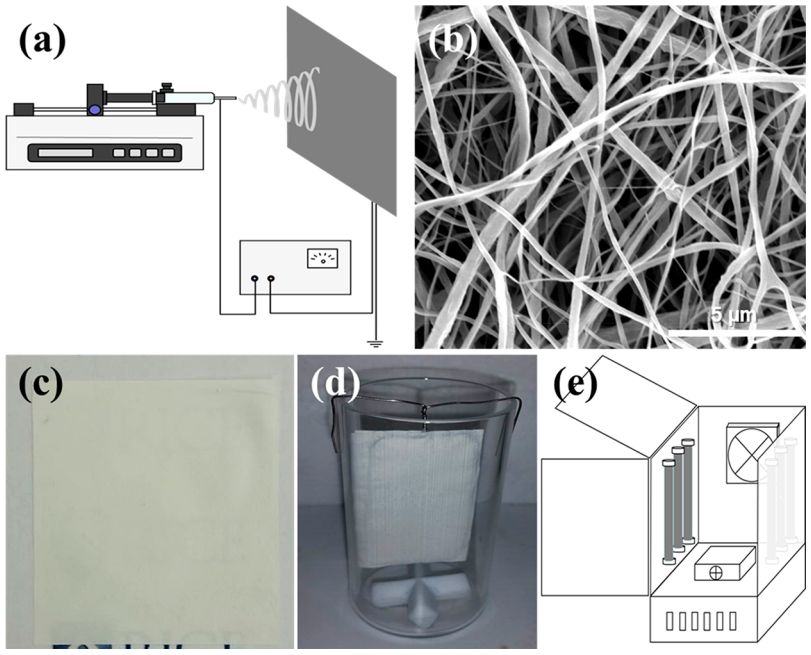


**Figure 1.** (a) Schematic of electrospinning process, (b) SEM image of electrospun porous fiber (EPF(2/1)-$TiO_2$), (c) coupon of fiber mat (4 × 5 $cm^2$), (d) quartz beaker with mounted coupons (50 mL), and (e) schematic diagram of photoreactor (18 × 18 × 18 $cm^3$).

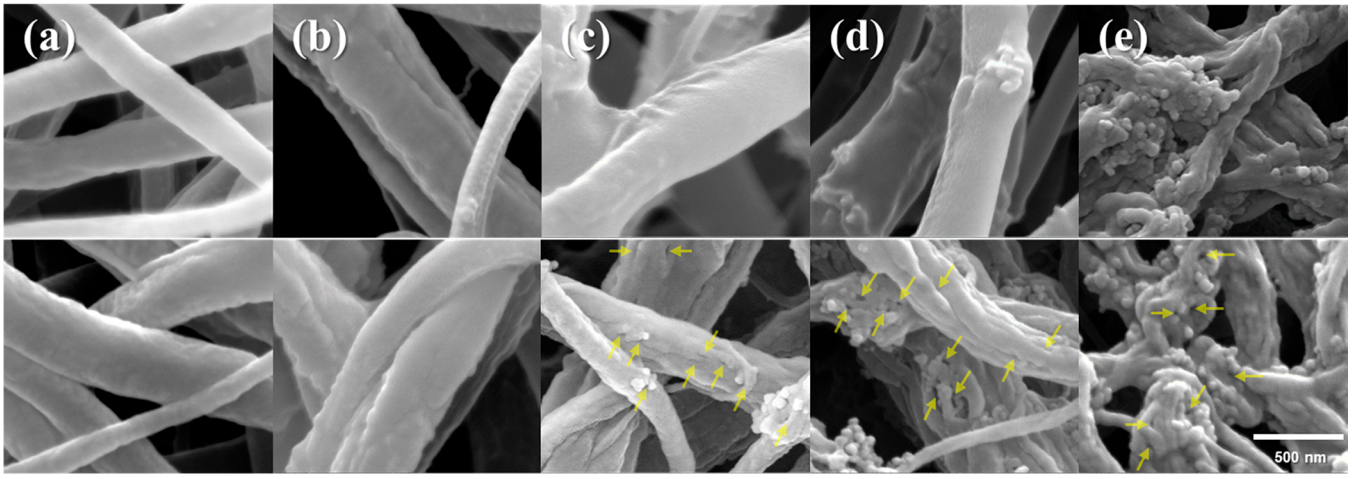


**Figure 2.** SEM image of the samples with different blending composition: (a) PVDF(18%), (b) PVDF(18%)-$TiO_2$, (c) PVDF(12%)/PVP(6%)-$TiO_2$, (d) PVDF(9%)/PVP(9%)-$TiO_2$, and (e) PVDF(6%)/PVP(12%)-$TiO_2$ (Top: before washing, Bottom: after washing. Arrows point to surface pores.

analyzed using a high performance liquid chromatograph (LC-20AT, Shimadzu, Japan) equipped with a C-18 column ($dC_{18}$ Column, Atlantis) and an UV−vis detector (SPD-M20A, Shimadzu, Japan) at the mobile phase (60% acetonitrile and 40% water) flow rate of 1.0 mL/min and injection volume of 40 μL. The $TiO_2$ content in the sample was determined using an inductively coupled plasma-optical emission spectrometer (ICP-OES) (Optima 4300 DV, PerkinElmer) after acid digestion (mixing 5 mL sample aliquot with 4 mL hydrofluoric acid and 8 mL sulfuric acid and further diluting to 50 mL with 2% nitric acid). The method detection limit (MDL) for Ti was 27 μg/L. The total organic carbon (TOC) was determined by TOC analyzer (TOC-$V_{CSH}$, Shimadzu, Japan). The size and zeta potential of $TiO_2$ particles (SI Table S2 and Figure S4) were determined by dynamic light scattering and phase analysis light scattering, respectively, with a Zen 3600 Zetasizer Nano (Malvern Instruments, UK).

Electrical energy per order (EEO), defined as the number of kilowatts-hour (kWh) of electrical energy required to remove the concentration of a pollutant (BPA or EE2) by 1 order of magnitude (90%) in one cubic meter of contaminated water, was calculated as follows:[37,38]

$$\mathrm{EEO(kWh/m^3/oder)} = \frac{E \times \left(\frac{t}{60}\right)}{V \times \log\left(\frac{C_0}{C}\right)}$$

where $E$ is defined here as the irradiance delivered from the light sources (kWh), $t$ is irradiation (or operation) time (min), $V$ is solution volume ($m^3$), $C_0$ and $C$ are the initial and time $t$ (min) concentrations of pollutant, respectively. This equation can be simplified by using pseudo first-order rate constant ($k$, $min^{-1}$):



DOI: 10.1021/acs.est.7b06508
Environ. Sci. Technol. 2018, 52, 4285−4293

Table 2. Surface Area and $TiO_2$ Content of Novel Photocatalytic Mats

| sample name | weight (mg)[a] | BET specific surface area ($m^2$/g) | total area ($m^2$) | total pore volume (cc/g) | $TiO_2$ content (mg) (and wt %) |
|---|---|---|---|---|---|
| EF | 21.2 | 80.65 | 1.71 | 0.12 | |
| EF-$TiO_2$ | 87.5 | 47.33 | 4.14 | 0.16 | 20.7 (23.7%)[b] |
| EPF(2/1)-$TiO_2$ | 95.7 | 117.15 | 11.21 | 0.37 | 24.8 (25.9%) |
| EPF(1/1)-$TiO_2$ | 28.6 | 119.76 | 3.43 | 0.68 | 7.9 (27.7%) |

[a]The dimensions of the electrospun polymer mats were 4 cm × 5 cm. [b]Numbers in parentheses are percentage of mat dry weight.

$$\mathrm{EEO(kWh/m^3/oder)} = \frac{E}{V \times 60 \times 0.4343 \times k}$$

The $k$ values with their respective standard errors were estimated by fitting the data to first order kinetics. One tailed $t$ test was used to determine statistically significant differences between treatments at the 95% confidence level ($p < 0.05$).

## RESULTS AND DISCUSSION

**Blending Composition Affects Surface Morphology and Hydrophobicity of Electrospun Porous Fiber Mat.** The morphology of the EF/EPF mats was affected by both the type of polymers used and their blending ratio. The nonporous EF mats (i.e., before removing PVP by washing) had a smooth surface (Figure 2, top row), except for the sample with the blending ratio of PVDF(6%)/PVP(12%). The bead-like structures on this sample with the highest PVP content likely indicate PVP aggregation (Figure 2(e)). The PVDF-only EFs had a diameter of 270 ± 200 nm (Figure 2(a)). Adding $TiO_2$ and PVP and subsequent washing of sacrificial PVP resulted in rougher surface morphology (Figure 2(b)−(d), bottom row). EF-$TiO_2$ (i.e., PVDF(18%)-$TiO_2$, Figure 2(b)), EPF(2/1)-$TiO_2$ (i.e., PVDF(12%)/PVP(6%)-$TiO_2$, Figure 2(c)), and EPF(1/1)-$TiO_2$ (i.e., PVDF(9%)/PVP(9%)-$TiO_2$, Figure 2(d)) had diameters of 1390 ± 520 nm, 440 ± 190 nm, and 260 ± 80 nm, respectively (SI Figure S5). The most robust and thickest mat (79.57 ± 9.04 μm) (SI Figure S6) was produced with EPF(2/1)-$TiO_2$. Thermogravimetric analysis (Figure S1) suggests that the $TiO_2$ content of this mat was 1.24 mg/$cm^2$ (26 wt % of the mat dry weight; Table 2).

The water contact angles (107.7 ± 7.3°; SI Figure S7) of the EPF mats were lower than those reported for super hydrophobic PVDF−$SiO_2$ electrospun nanofibers (160.5 ± 2.3°), but higher than those measured on a $TiO_2$/PVDF nanocomposite membrane (60.7 ± 0.4°).[39,40] There was no significant difference in contact angles between the fiber mats synthesized under different solution compositions ($p = 0.09$). Similar results have been reported for polyamide-12 and poly(methyl methacrylate) (PMMA) electrospun nanocomposite, where $TiO_2$ addition did not significantly affected the contact angle.[30,31]

**Fiber Pores Introduced by Sacrificial Removal of PVP Increased Surface Area and Access to $TiO_2$.** PVP removal by washing (to convert EF mats to EPF mats) significantly increased the BET surface area (e.g., from 30.6 to 117.2 $m^2$/g for EPF(2/1)-$TiO_2$; Table 2) through generation of internal pores in the fibers (Figure 2(c,d) bottom row, and Figure 3(a)). These values were much higher than previously reported for electrospun fiber mats (12.5 to 48.5 $m^2$/g)[27,41,42] likely due to pore generation. These values are also larger than the specific surface area of unbound $TiO_2$ (61.8 $m^2$/g; Table 2). We postulate that molecular weight difference between PVDF (MW = 534 000) and PVP (MW = 40 000) contributed to their facile separation.[23,43] Consistently, increasing the PVP content of the electrospinning solution also significantly increased the pore volume per unit weight of the fiber mat; i.e., from 0.37 cc/g for EPF(2/1)-$TiO_2$ (PVDF:PVP = 2:1) to 0.68 cc/g for EPF(1/1)-$TiO_2$ (PVDF:PVP = 1:1) (Table 2; SI Figures S8−S11). Furthermore, TEM analysis showed that $TiO_2$ (Figure 3(b), arrows) was present in the interior of the fiber throughout its diameter.

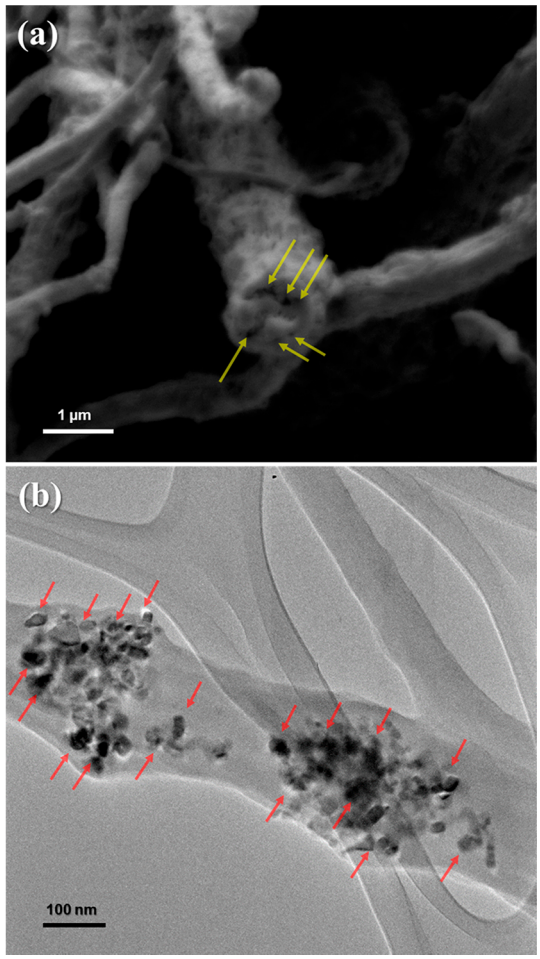


Figure 3. (a) Cross section SEM image of EPF(2/1)-$TiO_2$ mat showing fiber internal pores (yellow arrows) and (b) TEM image of electrospun porous fiber containing nanoscale $TiO_2$. (red arrows).

**Sorption Capacity, Photocatalytic Activity and Reusability of $TiO_2$ Electrospun Mats.** Both EPF(2/1)-$TiO_2$ and EF-$TiO_2$ mats effectively adsorbed MB under dark conditions (Figure 4(a)). While MB (log $K_{ow}$ = 5.85) is known to adsorb on hydrophobic surfaces such as PVDF,[6,44] the EF mat made of pristine PVDF (without pores and $TiO_2$) adsorbed only 14.7 ± 0.5% of the added MB. The maximum MB adsorption capacity of EPF(2/1)-$TiO_2$ was 5.93 ± 0.23 mg/g based on Langmuir isotherm analysis (SI Figure S12 and Table S3).


DOI: 10.1021/acs.est.7b06508
Environ. Sci. Technol. 2018, 52, 4285−4293

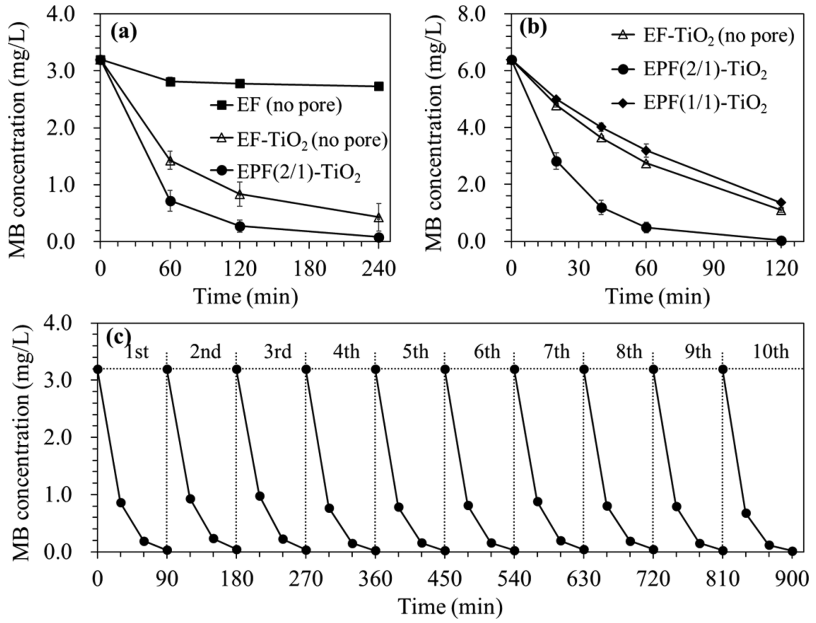


**Figure 4.** (a) Adsorption of methylene blue ($[MB]_0$ = 3.2 mg/L) under dark conditions using mats made with electrospun fiber (EF), electrospun nonporous fiber containing P25 $TiO_2$ (EF- $TiO_2$), or electrospun porous fiber containing $TiO_2$ (EPF(2/1)-$TiO_2$) (fiber pores were generated by polymer blending with PVDF(12%) and PVP(6%), and subsequent washing of PVP); (b) Removal of MB ($[MB]_0$ = 6.4 mg/L) by concurrent adsorption and photocatalytic degradation under UVA irradiation ($3.64 \times 10^{-9}$ einstein/$cm^2$/s) using mats made with EF-$TiO_2$ or electrospun porous fibers prepared with different polymer blending ratio (EPF(2/1)-$TiO_2$: PVDF(12%)/PVP(6%) and EPF(1/1)-$TiO_2$: PVDF(9%)/PVP(9%)); (c) Reuse of EPF(2/1)-$TiO_2$ mat over 10 cycles to remove methylene blue ($[MB]_0$ = 3.2 mg/L) under similar irradiation conditions.

Photocatalytic degradation tests (Figure 4(b)) showed a sharp decrease in the concentration of solution phase MB during treatment by EPF(2/1)-$TiO_2$ under UVA irradiation, with first-order rate constant, $k = 0.044 \pm 0.006$ $min^{-1}$. This removal (under conditions that allow for simultaneous MB sorption and photocatalytic degradation) was significantly faster than MB removal in the presence of EF-$TiO_2$ without pores ($k = 0.015 \pm 0.0004$ $min^{-1}$) or porous EPF(1/1)-$TiO_2$ ($k = 0.013 \pm 0.001$ $min^{-1}$). The fiber diameter (SI Figure S5) could also affect the photocatalytic reactivity because smaller diameters facilitate light penetration and mass transfer. Despite the thinner fiber diameter and higher porosity of EPF (1/1)-$TiO_2$ (Table 2), EPF(2/1)-$TiO_2$ exerted a higher removal rate apparently due to its thicker mat (80 vs 51 $\mu$m) with higher total surface area and $TiO_2$ content (Table 2). The EPF(2/1)-$TiO_2$ fiber also retained this first-order removal rate constant over the 10 cycles of concurrent sorption and photocatalytic degradation ($k = 0.050 \pm 0.004$ $min^{-1}$, which is indiscernible from the original value, $p < 0.05$) (Figure 4(c)). Over these 10 cycles there was no change in MB adsorption capacity, nor photocatalytic degradation rate, which implies that neither MB nor MB byproducts remained on the mat at significant levels between bait-hook-destroy cycles. Furthermore, ICP-OES analysis did not detect titanium leaching from the material into the water (detection limit 27 $\mu$g/L) and FT-IR analysis did not show changes in functional groups (878 (C−F), 1177 (C−C), 1401 ($CH_2$) $cm^{-1}$)[45] of the EPF(2/1)-$TiO_2$ mat surface over these 10 cycles (SI Figure S13), suggesting that PVDF is robust for use in photocatalytic treatment. This is corroborated by water contact angle measurements (to assess potential changes in hydrophobicity due to polymer oxidation), which remained relatively constant (SI Figure S7).

**Bait-Hook-and-Destroy Strategy for Contaminant Removal.** Simultaneous adsorption ("bait-hook") and photocatalytic degradation ("destroy"), as described above for MB removal, can be advantageous to treat relatively clear water that does not hinder UV penetration. This would accomplish efficient utilization of oxidation capacity to eliminate priority organic pollutants that concentrate near photoactive sites, with simultaneous mat regeneration in a single step. The bait-hook and destroy strategy can also be used to treat turbid wastewaters that hinder light penetration, by uncoupling the adsorption and photocatalytic degradation stages; that is, perform the latter separately under more favorable higher-transmittance conditions. To demonstrate this approach, the EPF(2/1)-$TiO_2$ mat was first used to adsorb MB (3.2 mg/L) in the dark, and then degrade it (with concomitant mat regeneration) under UV irradiation in DI water. About 97% of the MB was sorbed within 240 min (Figure 5: images 1 and 2), and subsequent UV irradiation completely removed the adsorbed contaminant in less than 90 min (Figure 5: images 3 to 5).

**Application of $TiO_2$ Electrospun Mats for EDC Degradation.** The EPF(2/1)-$TiO_2$ mat achieved greater than 96% removal efficiency for BPA and EE2 in DI water within 4 and 1.5 h, respectively (SI Figure S14, $C_0$ = 5.0 mg/L), under concomitant sorption and photocatalytic degradation. The $k$ values for BPA and EE2 removal were $0.030 \pm 0.004$ and $0.033 \pm 0.006$ $min^{-1}$, respectively, which are comparable to values reported in the literature (Table 3).[46−48] Note that removal of these compounds was mainly due to photocatalytic activity since adsorption under dark conditions was relatively small (i.e., 5% for BPA and 11% for EE2 of amount removed in 2 h) (SI Figure S15). For experiments conducted with 2× different initial MB concentrations the $k$ values decreased slightly but were not statistically different ($p < 0.05$).

In the presence of background organic matter (WWTP effluent with TOC = $17.11 \pm 0.23$ mg/L; SI Table S1), the removal rate of BPA by EPF(2/1)-$TiO_2$ decreased by 52%, but to a much lesser extent compared to suspended $TiO_2$ (91%).



DOI: 10.1021/acs.est.7b06508
Environ. Sci. Technol. 2018, 52, 4285−4293

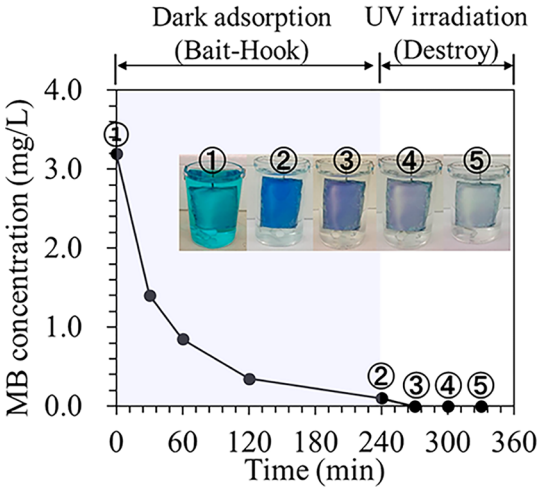


**Figure 5.** Uncoupling sorption of methylene blue ($[MB]_0$ = 10 $\mu$M) under dark conditions (240 min) and subsequent mat regeneration (with photocatalytic degradation of MB) by UV-A irradiation (3.64 × $10^{-9}$ einstein/$cm^2$/s) (90 min). This mat was made with electrospun porous fiber containing P25 $TiO_2$ (EPF(2/1)-$TiO_2$).

For this comparison, we used a slurry of $TiO_2$ (30 mg/L) that exerted a similar BPA removal rate as the EPF(2/1)-$TiO_2$ mat in DI water ($k$ = 0.030 ± 0.002 $min^{-1}$). Note that this mat was loaded with $TiO_2$ at an equivalent suspended concentration of 496 mg/L, which reflects the known loss of $TiO_2$ activity upon immobilization (SI Figure S16).[2,23] Nevertheless, this is compensated by the fact that the photocatalytic mat was less susceptible than $TiO_2$ slurry to inhibition by background organic matter that commonly scavenges ROS and electron holes, as well as by the capability of easy reuse. Incidentally, the irradiated EPF(2/1)-$TiO_2$ mat removed 16% of the background TOC in 2 h (data not shown).

Another advantage of $TiO_2$ immobilization is potential energy savings, which is a major factor determining the feasibility of photocatalytic treatment.[2,5,6] Although EEO values are reactor specific,[49,50] our calculations show that the EPF(2/1)-$TiO_2$ mat could remove BPA from WWTP effluents with lower energy requirements than the $TiO_2$ slurry, even if we ignore the energy requirements for slurry separation by membrane filtration, which could be significantly greater than the energy required to power the UV lamps.[50,51] Comparing the increase in energy requirement associated with loss of efficiency for BPA degradation in WWTP effluent, the EEO was 2.1-fold higher for the EPF(2/1)-$TiO_2$ mat (from 2.3 kWh/$m^3$/order in DI water to 4.9 kWh/$m^3$/order in WWTP effluent), versus a 11-fold increase for the $TiO_2$ slurry (from 2.3 kWh/$m^3$/order in DI water to 24.7 kWh/$m^3$/order in WWTP effluent) (Figure 6(c,d)). For reference, EEO values for "viable" photocatalytic treatment typically range from 0.1 to 100 kWh/$m^3$/order, depending on the targeted pollutant and reactor configuration.[50,52] Thus, our findings unequivocally show that the mat is more effective and more energy efficient than the slurry for the photocatalytic degradation of these types of trace organics present in secondary effluent (Figure 6).

**Implications for Water Treatment.** This novel $TiO_2$-embedded PVDF fiber mat offers several potential advantages over conventional $TiO_2$ slurry systems: (1) it does not require energy-intensive separation process, which is essential not only to easily reuse $TiO_2$ but to prevent unwanted release of $TiO_2$ into the treated water; (2) its hydrophobic surface facilitates adsorption and concentration of nonpolar organic contaminants near photocatalytic sites; and (3) it can be readily regenerated even when treating turbid wastewaters if photocatalysis is uncoupled from adsorption. The simultaneous or sequential "bait-hook and destroy" strategy is important to make the mat less susceptible to interference from coexisting water constituents such as ROS-scavenging dissolved organics

**Table 3. Comparison of Photocatalytic Contaminants Removal Rate by Immobilized $TiO_2$ on Different Substrates**

| target compound | catalyst | substrate | light source | loading | initial target concentration | removal rate | reference |
|---|---|---|---|---|---|---|---|
| MB | $TiO_2$ | PVDF | $\lambda$ = 350–400 nm (4 W) | 20 $cm^2$/50 mL | 10 $\mu$M | 0.0502 ± 0.0036 $min^{-1}$ | this study |
| | | | | | 20 $\mu$M | 0.0435 ± 0.0055 $min^{-1}$ | |
| | $TiO_2$ | PMMA | $\lambda$ = 254 nm (8 W) | 9 $cm^2$/50 mL | 31.3 $\mu$M | 0.0013 $min^{-1}$ | Koysuren and Koysuren, 2017 |
| | $TiO_2$ | PMMA | $\lambda$ = 365 nm (8 W) | 25 $cm^2$/50 mL | 6.25 $\mu$M | 0.0300 $min^{-1}$ | Vild et al., 2016 |
| | $TiO_2$ | P(VDF-TrFE) | $\lambda$ = 365 nm (4 mW/$cm^2$) | 12 $cm^2$/13 mL | 10 $\mu$M | 0.0220 $min^{-1}$ | Almeida et al., 2016 |
| | $TiO_2$/GO | | | | | 0.0280 $min^{-1}$ | |
| | Ag-$TiO_2$ | nylon-6,6 | $\lambda$ = 380–480 nm | | | 0.0035 $min^{-1}$ | Ryu et al., 2015 |
| | $TiO_2$ | polyamide-12 | $\lambda$ = 365 nm (5 mW/$cm^2$) | 12.25 $cm^2$/13 mL | 10 $\mu$M | 0.0116 $min^{-1}$ | Cossich et al., 2015 |
| BPA | $TiO_2$ | PVDF | $\lambda$ = 350–400 nm (4 W) | 20 $cm^2$/50 mL | 21.9 $\mu$M | 0.0296 ± 0.0041 $min^{-1}$ | this study |
| | $TiO_2$ | PVDF | $\lambda$ = 350–400 nm (4 W) | 22.5 $cm^2$/45 mL | 10 $\mu$M | 0.0361 $min^{-1}$ | Ramasundaram et al., 2015 |
| | $TiO_2$ | chitosan/PVA | $\lambda$ = 352–368 nm (10 W) | 0.2 g/1,000 mL | 43.8 $\mu$M | 0.0159 $min^{-1}$ | Yun et al., 2016 |
| EE2 | $TiO_2$ | PVDF | $\lambda$ = 350–400 nm (4 W) | 20 $cm^2$/50 mL | 16.9 $\mu$M | 0.0326 ± 0.0063 $min^{-1}$ | this study |
| | $TiO_2$ | glass beads | $\lambda$ = 365 nm (4 W) | 13.6 g/15 mL | 1 $\mu$M | 0.0045 $min^{-1}$ | Mizuguchi et al., 2006 |
| | $TiO_2$/$WO_3$ | glass-FTO | | 1 $cm^2$/10 mL | 33.7 $\mu$M | 0.0052 $min^{-1}$ | Oliveira et al., 2015 |



DOI: 10.1021/acs.est.7b06508
Environ. Sci. Technol. 2018, 52, 4285–4293

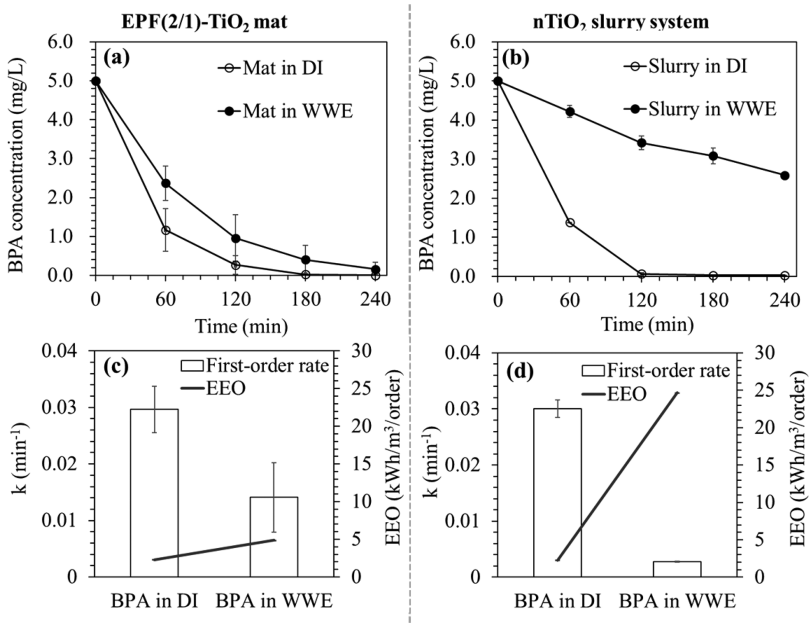


**Figure 6.** Photocatalytic degradation of bisphenol A (BPA) using electrospun porous fiber containing P25 $TiO_2$ (EPF(2/1)-$TiO_2$) (a, c) versus suspended $TiO_2$ (30 mg/L) (b, d). Bars depict first-order rate constants, and continuous line shows energy consumption per electrical-energy-per-order-of-reaction (EEO) values. Experiments were conducted in deionized water (DI) and wastewater treatment plant effluent (WWE) (TOC = 17 mg/L) with BPA (5 mg/L).

compounds, which can lead to further energy savings associated with more efficient utilization of UV irradiation. Further improvements such as more efficient $TiO_2$ anchoring on the surface of porous fibers (rather than inside the polymer matrix), better dispersion of $TiO_2$ as a primary particle (rather than aggregates) across the fibers, and advanced pore architecture (e.g., control of pore size and volume) would make this approach more appealing for practical applications in water treatment and reuse efforts.

## ■ ASSOCIATED CONTENT

### Supporting Information

The Supporting Information is available free of charge on the ACS Publications website at DOI: 10.1021/acs.est.7b06508.

Additional data included in the SI section include thermogravimetric analysis, water contact angles, surface area analysis with pore distribution curves, and FT-IR spectrum of electrospun fiber mats; chemical actinometry; and MB adsorption isotherm (PDF)

## ■ AUTHOR INFORMATION


### Corresponding Author

*Phone: +1 713 348 5903; e-mail: alvarez@rice.edu.

### ORCID

Jae-Hong Kim: 0000-0003-2224-3516

Paul Westerhoff: 0000-0002-9241-8759

Qilin Li: 0000-0001-5756-3873

Pedro J. J. Alvarez: 0000-0002-6725-7199

### Present Addresses

[⊥](C.-G.L.) Department of Environmental and Safety Engineering, Ajou University, Suwon, South Korea.

[¶](H.J.) Department of Chemistry, Rice University, Houston, Texas 77005, United States.


### Notes

The authors declare no competing financial interest.

## ■ ACKNOWLEDGMENTS

This work was partially funded by the National Science Foundation (EEC-1449500) Nanosystems Engineering Research Center on Nanotechnology-Enabled Water Treatment (NEWT).

## ■ REFERENCES


(1) Park, H.; Park, Y.; Kim, W.; Choi, W. Surface modification of TiO2 photocatalyst for environmental applications. *J. Photochem. Photobiol., C* **2013**, *15*, 1−20.

(2) Dong, H.; Zeng, G.; Tang, L.; Fan, C.; Zhang, C.; He, X.; He, Y. An overview on limitations of TiO2-based particles for photocatalytic degradation of organic pollutants and the corresponding counter-measures. *Water Res.* **2015**, *79*, 128−46.

(3) Hu, L.; Flanders, P. M.; Miller, P. L.; Strathmann, T. J. Oxidation of sulfamethoxazole and related antimicrobial agents by TiO2 photocatalysis. *Water Res.* **2007**, *41* (12), 2612−26.

(4) Pelaez, M.; Nolan, N. T.; Pillai, S. C.; Seery, M. K.; Falaras, P.; Kontos, A. G.; Dunlop, P. S. M.; Hamilton, J. W. J.; Byrne, J. A.; O'Shea, K.; Entezari, M. H.; Dionysiou, D. D. A review on the visible light active titanium dioxide photocatalysts for environmental applications. *Appl. Catal., B* **2012**, *125*, 331−349.

(5) Singh, S.; Mahalingam, H.; Singh, P. K. Polymer-supported titanium dioxide photocatalysts for environmental remediation: A review. *Appl. Catal., A* **2013**, *462*, 178−195.

(6) He, T.; Zhou, Z.; Xu, W.; Ren, F.; Ma, H.; Wang, J. Preparation and photocatalysis of TiO2−fluoropolymer electrospun fiber nanocomposites. *Polymer* **2009**, *50* (13), 3031−3036.

(7) Zhang, Y.; Chen, Y.; Westerhoff, P.; Hristovski, K.; Crittenden, J. C. Stability of commercial metal oxide nanoparticles in water. *Water Res.* **2008**, *42* (8−9), 2204−12.

(8) Brame, J.; Long, M.; Li, Q.; Alvarez, P. Trading oxidation power for efficiency: differential inhibition of photo-generated hydroxyl radicals versus singlet oxygen. *Water Res.* **2014**, *60*, 259−66.

(9) Giannakis, S.; Liu, S.; Carratala, A.; Rtimi, S.; Talebi Amiri, M.; Bensimon, M.; Pulgarin, C. Iron oxide-mediated semiconductor photocatalysis vs. heterogeneous photo-Fenton treatment of viruses in wastewater. Impact of the oxide particle size. *J. Hazard. Mater.* **2017**, *339*, 223−231.




DOI: 10.1021/acs.est.7b06508
*Environ. Sci. Technol.* 2018, 52, 4285−4293

(10) Gao, B.; Peng, C.; Chen, G.; Lipuma, G. Photo-electro-catalysis enhancement on carbon nanotubes/titanium dioxide (CNTs/TiO2) composite prepared by a novel surfactant wrapping sol−gel method. *Appl. Catal., B* **2008**, *85* (1−2), 17−23.
(11) Deng, F.; Lu, X.; Pei, X.; Luo, X.; Luo, S.; Dionysiou, D. D. Fabrication of ternary reduced graphene oxide/SnS2/ZnFe2O4 composite for high visible-light photocatalytic activity and stability. *J. Hazard. Mater.* **2017**, *332*, 149−161.
(12) Huang, A.; Wang, N.; Lei, M.; Zhu, L.; Zhang, Y.; Lin, Z.; Yin, D.; Tang, H. Efficient oxidative debromination of decabromodiphenyl ether by TiO2-mediated photocatalysis in aqueous environment. *Environ. Sci. Technol.* **2013**, *47* (1), 518−25.
(13) Chen, P.; Zhu, L.; Fang, S.; Wang, C.; Shan, G. Photocatalytic degradation efficiency and mechanism of microcystin-RR by mesoporous Bi(2)WO(6) under near ultraviolet light. *Environ. Sci. Technol.* **2012**, *46* (4), 2345−51.
(14) Lee, J.; Hong, S.; Mackeyev, Y.; Lee, C.; Chung, E.; Wilson, L. J.; Kim, J. H.; Alvarez, P. J. Photosensitized oxidation of emerging organic pollutants by tetrakis C(6)(0) aminofullerene-derivatized silica under visible light irradiation. *Environ. Sci. Technol.* **2011**, *45* (24), 10598−604.
(15) Xiang, Q.; Yu, J.; Jaroniec, M. Synergetic effect of MoS2 and graphene as cocatalysts for enhanced photocatalytic H2 production activity of TiO2 nanoparticles. *J. Am. Chem. Soc.* **2012**, *134* (15), 6575−8.
(16) Zhang, P.; Yang, X.; Zhao, Z.; Li, B.; Gui, J.; Liu, D.; Qiu, J. One-step synthesis of flowerlike C/Fe 2 O 3 nanosheet assembly with superior adsorption capacity and visible light photocatalytic performance for dye removal. *Carbon* **2017**, *116*, 59−67.
(17) Luo, X.; Deng, F.; Min, L.; Luo, S.; Guo, B.; Zeng, G.; Au, C. Facile one-step synthesis of inorganic-framework molecularly imprinted TiO2/WO3 nanocomposite and its molecular recognitive photocatalytic degradation of target contaminant. *Environ. Sci. Technol.* **2013**, *47* (13), 7404−12.
(18) Jafry, H. R.; Liga, M. V.; Li, Q.; Barron, A. R. Simple route to enhanced photocatalytic activity of p25 titanium dioxide nanoparticles by silica addition. *Environ. Sci. Technol.* **2011**, *45* (4), 1563−8.
(19) Shan, A. Y.; Ghazi, T. I. M.; Rashid, S. A. Immobilisation of titanium dioxide onto supporting materials in heterogeneous photocatalysis: A review. *Appl. Catal., A* **2010**, *389* (1−2), 1−8.
(20) Zhang, G.; Yi, J.; Shim, J.; Lee, J.; Choi, W. Photocatalytic hydroxylation of benzene to phenol over titanium oxide entrapped into hydrophobically modified siliceous foam. *Appl. Catal., B* **2011**, *102* (1−2), 132−139.
(21) Carbonaro, S.; Sugihara, M. N.; Strathmann, T. J. Continuous-flow photocatalytic treatment of pharmaceutical micropollutants: Activity, inhibition, and deactivation of TiO2 photocatalysts in wastewater effluent. *Appl. Catal., B* **2013**, *129*, 1−12.
(22) Lemal, D. M. Perspective on fluorocarbon chemistry. *J. Org. Chem.* **2004**, *69* (1), 1−11.
(23) Hoogesteijn von Reitzenstein, N.; Bi, X.; Yang, Y.; Hristovski, K.; Westerhoff, P. Morphology, structure, and properties of metal oxide/polymer nanocomposite electrospun mats. *J. Appl. Polym. Sci.* **2016**, *133* (33), 43811−9.
(24) Ramasundaram, S.; Son, A.; Seid, M. G.; Shim, S.; Lee, S. H.; Chung, Y. C.; Lee, C.; Lee, J.; Hong, S. W. Photocatalytic applications of paper-like poly(vinylidene fluoride)-titanium dioxide hybrids fabricated using a combination of electrospinning and electrospraying. *J. Hazard. Mater.* **2015**, *285*, 267−76.
(25) Bognitzki, M.; Czado, W.; Frese, T.; Schaper, A.; Hellwig, M.; Steinhart, M.; Greiner, A.; Wendorff, J. H. Nanostructured fibers via electrospinning. *Adv. Mater.* **2001**, *13* (1), 70−72.
(26) Nasir, M.; Matsumoto, H.; Minagawa, M.; Tanioka, A.; Danno, T.; Horibe, H. Preparation of Porous PVDF Nanofiber from PVDF/PVP Blend by Electrospray Deposition. *Polym. J.* **2007**, *39* (10), 1060−1064.
(27) Ning, J.; Yang, M.; Yang, H.; Xu, Z. Tailoring the morphologies of PVDF nanofibers by interfacial diffusion during coaxial electrospinning. *Mater. Des.* **2016**, *109*, 264−269.
(28) Prahsarn, C.; Klinsukhon, W.; Roungpaisan, N. Electrospinning of PAN/DMF/H2O containing TiO2 and photocatalytic activity of their webs. *Mater. Lett.* **2011**, *65* (15−16), 2498−2501.
(29) Guan, J.; Li, J.; Li, Y. Electrospun nanofibers with both surface nanopores and internal interpenetrated nanochannels for oil absorption. *RSC Adv.* **2016**, *6* (40), 33781−33788.
(30) Vild, A.; Teixeira, S.; Kühn, K.; Cuniberti, G.; Sencadas, V. Orthogonal experimental design of titanium dioxide—Poly(methyl methacrylate) electrospun nanocomposite membranes for photocatalytic applications. *J. Environ. Chem. Eng.* **2016**, *4* (3), 3151−3158.
(31) Cossich, E.; Bergamasco, R.; Pessoa de Amorim, M. T.; Martins, P. M.; Marques, J.; Tavares, C. J.; Lanceros-Méndez, S.; Sencadas, V. Development of electrospun photocatalytic TiO2-polyamide-12 nanocomposites. *Mater. Chem. Phys.* **2015**, *164*, 91−97.
(32) Almeida, N. A.; Martins, P. M.; Teixeira, S.; Lopes da Silva, J. A.; Sencadas, V.; Kühn, K.; Cuniberti, G.; Lanceros-Mendez, S.; Marques, P. A. A. P. TiO2/graphene oxide immobilized in P(VDF-TrFE) electrospun membranes with enhanced visible-light-induced photocatalytic performance. *J. Mater. Sci.* **2016**, *51* (14), 6974−6986.
(33) Ryu, S.-Y.; Chung, J. W.; Kwak, S.-Y. Dependence of photocatalytic and antimicrobial activity of electrospun polymeric nanofiber composites on the positioning of Ag−TiO 2 nanoparticles. *Compos. Sci. Technol.* **2015**, *117*, 9−17.
(34) Koysuren, O.; Koysuren, H. N. Photocatalytic activities of poly(methyl methacrylate)/titanium dioxide nanofiber mat. *J. Macromol. Sci., Part A: Pure Appl.Chem.* **2017**, *54* (2), 80−84.
(35) An, S.; Lee, M. W.; Joshi, B. N.; Jo, A.; Jung, J.; Yoon, S. S. Water purification and toxicity control of chlorophenols by 3D nanofiber membranes decorated with photocatalytic titania nanoparticles. *Ceram. Int.* **2014**, *40* (2), 3305−3313.
(36) Bolton, J. R.; Stefan, M. I.; Shaw, P.-S.; Lykke, K. R. Determination of the quantum yields of the potassium ferrioxalate and potassium iodide−iodate actinometers and a method for the calibration of radiometer detectors. *J. Photochem. Photobiol., A* **2011**, *222* (1), 166−169.
(37) Lanzarini-Lopes, M.; Garcia-Segura, S.; Hristovski, K.; Westerhoff, P. Electrical energy per order and current efficiency for electrochemical oxidation of p-chlorobenzoic acid with boron-doped diamond anode. *Chemosphere* **2017**, *188*, 304−311.
(38) Daneshvar, N.; Aleboyeh, A.; Khataee, A. R. The evaluation of electrical energy per order (E(Eo)) for photooxidative decolorization of four textile dye solutions by the kinetic model. *Chemosphere* **2005**, *59* (6), 761−7.
(39) Moghadam, M. T.; Lesage, G.; Mohammadi, T.; Mericq, J. P.; Mendret, J.; Heran, M.; Faur, C.; Brosillon, S.; Hemmati, M.; Naeimpoor, F. Improved antifouling properties of TiO2/PVDF nanocomposite membranes in UV-coupled ultrafiltration. *J. Appl. Polym. Sci.* **2015**, *132* (21), 41731−13.
(40) Dong, Z.-Q.; Ma, X.-H.; Xu, Z.-L.; Gu, Z.-Y. Superhydrophobic modification of PVDF−SiO 2 electrospun nanofiber membranes for vacuum membrane distillation. *RSC Adv.* **2015**, *5* (83), 67962−67970.
(41) Lolla, D.; Lolla, M.; Abutaleb, A.; Shin, H. U.; Reneker, D. H.; Chase, G. G. Fabrication, Polarization of Electrospun Polyvinylidene Fluoride Electret Fibers and Effect on Capturing Nanoscale Solid Aerosols. *Materials* **2016**, *9* (8), 671.
(42) Gebru, K. A.; Das, C. Removal of Pb (II) and Cu (II) ions from wastewater using composite electrospun cellulose acetate/titanium oxide (TiO 2) adsorbent. *Journal of Water Process Engineering* **2017**, *16*, 1−13.
(43) Huang, J.; You, T. Electrospun Nanofibers: From Rational Design, Fabrication to Electrochemical Sensing Applications. In *Advances in Nanofibers*; Maguire, R., Eds; InTech, 2013; pp 35.
(44) Buonomenna, M. G.; Lopez, L. C.; Favia, P.; d'Agostino, R.; Gordano, A.; Drioli, E. New PVDF membranes: The effect of plasma surface modification on retention in nanofiltration of aqueous solution containing organic compounds. *Water Res.* **2007**, *41* (19), 4309−16.
(45) Bai, H.; Wang, X.; Zhou, Y.; Zhang, L. Preparation and characterization of poly(vinylidene fluoride) composite membranes


DOI: 10.1021/acs.est.7b06508
*Environ. Sci. Technol.* 2018, 52, 4285−4293

blended with nano-crystalline cellulose. *Prog. Nat. Sci.* **2012**, *22* (3), 250−257.
(46) Yun, Y.-H.; Yun, J.-W.; Yoon, S.-D.; Byun, H.-S. Physical properties and photocatalytic activity of chitosan-based nanocomposites added titanium oxide nanoparticles. *Macromol. Res.* **2016**, *24* (1), 51−59.
(47) Mizuguchi, T.; Sadaka, S.; Ogasawara, C.; Shimada, K. Determination of the Effect of Hydrogen Peroxide on Photocatalytic Degradation of Estrogen Using HPLC. *J. Liq. Chromatogr. Relat. Technol.* **2006**, *29* (6), 903−911.
(48) Oliveira, H. G.; Ferreira, L. H.; Bertazzoli, R.; Longo, C. Remediation of 17-alpha-ethinylestradiol aqueous solution by photocatalysis and electrochemically-assisted photocatalysis using TiO2 and TiO2/WO3 electrodes irradiated by a solar simulator. *Water Res.* **2015**, *72*, 305−14.
(49) Beck, S. E.; Ryu, H.; Boczek, L. A.; Cashdollar, J. L.; Jeanis, K. M.; Rosenblum, J. S.; Lawal, O. R.; Linden, K. G. Evaluating UV-C LED disinfection performance and investigating potential dual-wavelength synergy. *Water Res.* **2017**, *109*, 207−216.
(50) Benotti, M. J.; Stanford, B. D.; Wert, E. C.; Snyder, S. A. Evaluation of a photocatalytic reactor membrane pilot system for the removal of pharmaceuticals and endocrine disrupting compounds from water. *Water Res.* **2009**, *43* (6), 1513−22.
(51) Cates, E. L. Photocatalytic Water Treatment: So Where Are We Going with This? *Environ. Sci. Technol.* **2017**, *51* (2), 757−758.
(52) Stancl, H. O. N.; Hristovski, K.; Westerhoff, P. Hexavalent Chromium Removal Using UV-TiO2/Ceramic Membrane Reactor. *Environ. Eng. Sci.* **2015**, *32* (8), 676−683.
(53) Qin, Y.; Cui, Y.; Tian, Z.; Wu, Y.; Li, Y. Synthesis of AG@AgCl Core-Shell Structure Nanowires and Its Photocatalytic Oxidation of Arsenic (III) Under Visible Light. *Nanoscale Res. Lett.* **2017**, *12* (1), 247.
(54) Lim, J.; Kim, H.; Alvarez, P. J.; Lee, J.; Choi, W. Visible Light Sensitized Production of Hydroxyl Radicals Using Fullerol as an Electron-Transfer Mediator. *Environ. Sci. Technol.* **2016**, *50* (19), 10545−10553.
(55) Senthilkumaar, S.; Porkodi, K.; Gomathi, R.; Manonmani, N. Sol−gel derived silver doped nanocrystalline titania catalysed photodegradation of methylene blue from aqueous solution. *Dyes Pigm.* **2006**, *69* (1), 22−30.


DOI: 10.1021/acs.est.7b06508
*Environ. Sci. Technol.* 2018, 52, 4285−4293